Supplemental material: Photoinduced Enhancement of Excitonic Order

Yuta Murakami,[1] Denis Golež,[1] Martin Eckstein,[2] and Philipp Werner[1]
[1]*Department of Physics, University of Fribourg, 1700 Fribourg, Switzerland*
[2]*Department of Physics, University of Erlangen-Nürnberg, 91058 Erlangen, Germany*
(Dated: December 8, 2017)

Effects of other phonon modes

In the main text, we have considered a single phonon branch which is coupled to the transfer integral between the electron bands. In a more realistic scenario, the system is coupled to multiple phonon branches, and the question we want to address here is whether or not this has a qualitative effect on the mechanism discussed in the main text. In the following, we first introduce another type of electron-phonon (el-ph) coupling, which has been pointed out in the recent LDA calculation of Ref. [1]. Then we demonstrate that, in order to see the enhancement of the EI order and the gap, one needs at least one phonon mode that is coupled to the transfer integral between the electron bands. Hence, the number of phonon modes does not influence the physics we discussed in the main text.

Based on LDA calculations in Ref. [1], it was pointed out that a phonon mode at 1THz modifies the hybridization between bands as well as the on-site energy (crystal field splitting). If a phonon mode only has the latter effect, its Hamiltonian can be described by

$$H_{\mathrm{el-ph},2} + \hat{H}_{\mathrm{ph},2} = g_2 \sum_i (\hat{b}^\dagger_{i,2} + \hat{b}_{i,2})(\hat{n}_{i,0} - \hat{n}_{i,1}) + \omega_2 \sum_i \hat{b}^\dagger_{i,2}\hat{b}_{i,2}. \quad (1)$$

We denote the corresponding creation operator by $\hat{b}^\dagger_{i,2}$, the coupling constant by g_2, the phonon frequency by ω_2, and we introduce $\lambda_2 \equiv 2g_2^2/\omega_2$. This Hamiltonian represents optical phonons coupled to the electrons through the difference in occupancy between the valence and conduction bands, which is a different type of el-ph coupling than the one considered in the main part. In the following, we denote the el-ph coupling in the main text as "type 1" and the one introduced above as "type 2". We note that in general a given phonon mode can exhibit these two types of couplings at the same time, but for simplicity in this study we assume that each phonon mode possesses only one of them.

The dynamics of the type 2 phonons can also be treated within the mean-field theory by introducing the mean phonon displacement $X_2(t) \equiv \langle \hat{b}^\dagger_{i,2}(t) + \hat{b}_{i,2}(t)\rangle$. The decoupling of the interaction term is discussed in the next section. The dynamics of the pseudo-spins (electrons) is described by Eq. (2) of the main text, where B^x_k and B^y_k are given by Eq. (3a) and Eq. (3b) in the main text, respectively, and

$$B^z_k(t) = 2\epsilon^z_k - U\Delta n(t) + 2g_2 X_2(t). \quad (2)$$

The equation of motion for the phonons is $\partial_t P_2(t) = -\omega_2 X_2(t) - 2g_2\Delta n(t)$ and $\partial_t X_2(t) = \omega_2 P_2(t)$.

Let us first note that we cannot expect the enhancement of the EI order with the second type of el-ph coupling only. In the mechanism explained in the main part, a cooperative effect between the massive phase mode and the Hartree shift was essential for the enhancement. However, the second type of el-ph coupling does not break the U(1) symmetry, thus the EI breaks the continuous symmetry and the phase mode remains massless. Therefore, the mechanism discussed in the main text does not work, which is numerically shown below.

In Fig. 1, we show the properties of collective amplitude oscillations and the photo-induced dynamics for the case with only the second type of phonons. Here we use as a reference the same parameters as in the main text, i.e. $\Delta_0 = -0.55$, $\Delta_1 = -2.45$, $\lambda_2 = 0$ and $U = 3$. We take $\omega_2 = 0.1$ and, for the pump pulse, $E(t) = E_0 \sin(\Omega t)\exp(-(t-t_{\mathrm{p}})^2/(2\sigma_{\mathrm{p}}^2))$ with $\Omega = 6$, $\sigma_{\mathrm{p}} = 3$ and $t_{\mathrm{p}} = 6$. In Fig. 1(a), we show $\chi^R_{11}(t)$. As in the case without phonons, this quantity oscillates with Δ_{EI} and its amplitude decays $\sim 1/t^{1.5}$. In Figs. 1(b-d), we show the time evolution of several observables after the pump pulse. The gap at $k = 0$ ($\Delta(k = 0, t)$), the excitonic order parameter ($|\phi|$), and the phonon displacement (X_2) are suppressed after the pulse. As we increase the pulse amplitude the suppression becomes larger. The gap shows oscillations with the frequency ω_2, which originate from the phonon dynamics, while the value of the order parameter is almost constant.

Now we discuss the effects of multiple phonon branches. First we note that in reality we do not need to consider many phonon branches, since in the experiment of Ref. [1], only three prominent modes at 1, 2, and 3 THz were observed, with a strong signal from the 1THz and 3THz modes and a weaker signal from the 2THz mode. Motivated by this, we only consider two phonon branches and set the phonon frequencies to mimic the 1 THz and 3 THz modes, which corresponds to $\omega_{0,a} = 0.015$ and $\omega_{0,b} = 0.045$, respectively. Unfortunately, the detailed properties of the el-ph couplings are not available in the literature. Therefore, we assumed that they are either of type 1 or type 2. We thus checked three cases, i.e. (type 1, type 1), (type 1, type 2) and (type 2, type 1). In all

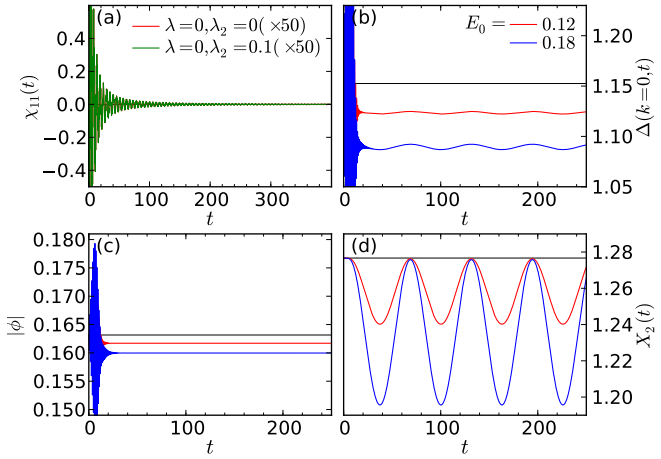

FIG. 1: (a) Susceptibility ($\chi^R_{11}(t)$) without phonons and with the type 2 phonons. The two curves are on top of each other. (b-d) Time evolution of the band gap at $k = 0$ ($\Delta(k = 0, t)$), the excitonic order parameter ($|\phi|$), and the phonon displacement (X_2) for various field strengths for $\lambda = 0, \lambda_2 = 0.1$. Vertical lines indicate the equilibrium values.

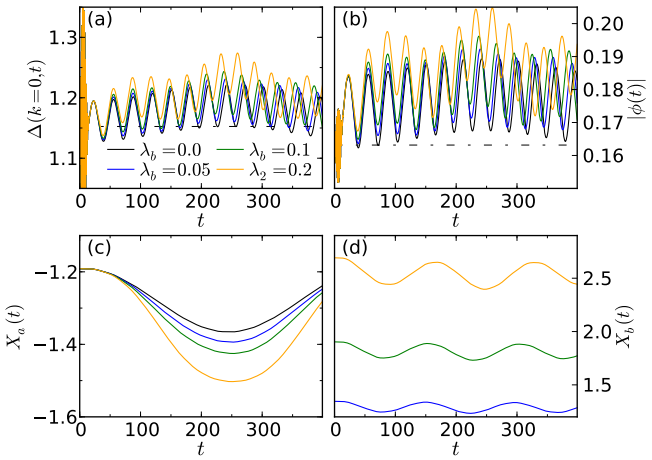

FIG. 2: Time evolution of the excitonic insulator with two phonon branches, Eq. (3). (a-d) Time evolution of the gap at $k = 0$, $\Delta(k = 0, t)$, the excitonic order parameter $|\phi|$, and the phonon displacement X_a and X_b for $\omega_{0,a} = 0.015$, $\omega_{0,b} = 0.045$, $\lambda_a = 0.1$, $E_0 = 0.12$, $T = 0$ and various λ_b (coupling strength of the type 2 phonon). We use $\Delta_0 = -0.55$, $\Delta_1 = -2.45$, $\lambda = 0$ and $U = 3$ as a reference as is discussed in the main text. The pump condition is the same as in the main text, $\Omega = 6$, $\sigma_{\rm p} = 3$. Vertical lines indicate the equilibrium values.

cases, we have confirmed that the enhancement of the EI order and the gap can be observed in a manner analogous to the single phonon branch set-up studied in the main text.

Here as a representative of these three cases we show the results of the case where the $\omega_{0,a}$ phonon is of type 1, while the $\omega_{0,b}$ phonon is of type 2. The Hamiltonian that includes these phonons explicitly reads

$$\begin{aligned} &H_{\rm el-ph} + H_{\rm ph} \\ &= g_a \sum_i (\hat{b}^\dagger_{i,a} + \hat{b}_{i,a})(\hat{c}^\dagger_{i,1}\hat{c}_{i,0} + \hat{c}^\dagger_{i,0}\hat{c}_{i,1}) + \omega_{0,a}\sum_i \hat{b}^\dagger_{i,a}\hat{b}_{i,a} \\ &+ g_b \sum_i (\hat{b}^\dagger_{i,b} + \hat{b}_{i,b})(\hat{n}_{i,0} - \hat{n}_{i,1}) + \omega_{0,b}\sum_i \hat{b}^\dagger_{i,b}\hat{b}_{i,b}, \end{aligned} \tag{3}$$

where $\hat{b}_{i,\gamma}$ is the annihilation operator for the phonon branch γ. We also introduce $\lambda_\gamma = 2g^2_\gamma/\omega_{0,\gamma}$. The electron part of the Hamiltonian is the same as in Eq. (1) of the main text.

In Fig. 2, we show the results for various sets of el-ph couplings. In all cases, we can see an enhancement of the EI gap and order parameter and the dynamics of $X_a(t)$ and $X_b(t)$ show that the main oscillation component is coming from $\omega_{0,a}$ and $\omega_{0,b}$, respectively. These results indicate that the frequency of the type 1 phonon does not affect the enhancement of the order (note that the frequency of the type 1 phonon used here is much smaller than the one used in the main text) and that the number of phonon branches is also irrelevant as far as at least one phonon is of type 1. One interesting observation here is that as we increase the coupling of the type 2 phonon, the enhancement of the EI gap and the EI order becomes larger. This can be explained as a positive feedback effect from the type 2 phonons. Since the phonon can move it can adjust its position to a more preferable point. In this case, because of the photo-doping, $|\Delta n(t)|$ first decreases and then the size of phonon displacement ($|X|$) becomes smaller. Because this phonon mode couples to the potential on each site, this yields a further reduction of the z component of the pseudo-magnetic field (B is more tilted towards the x axis.). This can further enhance the EI order.

Before we finish this section, we add some comments on 1) the effects of a phonon damping term and 2) the temperature dependence of the dynamics. To investigate point 1), we have introduced a damping term in the mean-field phonon dynamics, i.e. $\partial_t P(t) = -2\xi\omega_0 P(t) - \omega_0 X(t) - 4g{\rm Re}\phi(t)$ with ξ the damping factor. These calculations confirmed that even with a strong damping the enhancement of the order is realized after the pump. (It is important to note that the experiment shows that the oscillations after the pump are long-lived, hence in practice we do not need to worry about the phonon damping effects on the physics discussed in this paper.) As for 2), we have repeated the same calculations as in the main text for different initial temperatures. It turns out that, without the el-ph coupling, the order parameter and the gap decrease after the pulse at all temperatures, while with the el-ph coupling one can observe an enhancement up to temperatures very close to the thermal transition. Above the transition temperature, both cases show no enhancement of the order parameter and a suppression of the gap.

Mean-field theory

In the mean-field theory, at each time t, we decouple the interaction term as

$$\hat{n}_{i,0}\hat{n}_{i,1} \longrightarrow \tag{4}$$
$$\langle n_{i,0}(t)\rangle\hat{n}_{i,1} + \langle n_{i,1}(t)\rangle\hat{n}_{i,0} - \phi(t)\hat{c}^\dagger_{i,1}\hat{c}_{i,0} - \phi(t)^*\hat{c}^\dagger_{i,0}\hat{c}_{i1},$$

where the first two terms correspond to the Hartree terms and the latter two to the Fock terms. We also decouple the el-ph coupling terms as

$$(\hat{b}^\dagger_i + \hat{b}_i)(\hat{c}^\dagger_{i,1}c_{i,0} + \hat{c}^\dagger_{i,0}c_{i,1})$$
$$\to X(t)(\hat{c}^\dagger_{i,1}\hat{c}_{i,0} + \hat{c}^\dagger_{i,0}\hat{c}_{i,1}) + 2\mathrm{Re}\phi_0(t)(\hat{b}^\dagger_i + \hat{b}_i), \tag{5a}$$
$$(\hat{b}^\dagger_{i,2} + \hat{b}_{i,2})(\hat{n}_{i,0} - \hat{n}_{i,1})$$
$$\to X_2(t)(\hat{n}_{i,0} - \hat{n}_{i,1}) + (\hat{b}^\dagger_{i,2} + \hat{b}_{i,2})\Delta n(t). \tag{5b}$$

This decoupling is applicable for any systems with phonon branches of the type 1 or the type 2. In the following, we focus on the case where the electron part is coupled to one type 1 phonon branch and one type 2 phonon branch. Namely, the total Hamiltonian of the system is the sum of Eq. (1) in the main text and the above Eq. (1).

This leads to the mean-field Hamiltonians

$$H^{MF}_{\mathrm{el}}(t) = \frac{1}{2}\sum_k \hat{\Psi}^\dagger_k \begin{bmatrix} C^0_k + B^z_k(t) & B^x_k(t) - iB^y_k(t) \\ B^x_k(t) + iB^y_k(t) & C^0_k - B^z_k(t) \end{bmatrix} \hat{\Psi}_k$$
$$= \sum_{\mathrm{k}} \mathbf{B}_k(t)\cdot\hat{\mathbf{S}}_k + C^0_k\cdot\hat{I}_k, \tag{6a}$$

$$H^{\mathrm{MF}}_{\mathrm{ph0}}(t) = \omega_0\sum_i \hat{b}^\dagger_i\hat{b}_i + g(\phi(t)+\phi(t)^*)\sum_i \hat{X}_i, \tag{6b}$$

$$H^{\mathrm{MF}}_{\mathrm{ph2}}(t) = \omega_2\sum_i \hat{b}^\dagger_{i,2}\hat{b}_{i,2} + g_2\Delta n(t)\sum_i \hat{X}_{i,2}, \tag{6c}$$

where $\hat{X}_i = \hat{b}_i + \hat{b}^\dagger_i$, $\hat{X}_{i,2} = \hat{b}_{i,2} + \hat{b}^\dagger_{i,2}$ and

$$C^0_{\mathrm{k}} = (\epsilon_{k,0} + \epsilon_{k,1}) + (\Delta_0 + \Delta_1) + U(n_0 + n_1). \tag{7}$$

Here n_α indicates the number of electrons per site in the α band and $n_0 + n_1$ is constant. The equations of motion for observables shown in the main text are obtained from these mean-field Hamiltonians. By diagonalizing Eq. (6a) at each time, one can obtain the time-dependent (instantaneous) dispersion of the electrons, $E_\pm(k,t) \equiv (\pm|\mathrm{B}_k(t)| + C^0_k)/2$. Then the gap at each k ($\Delta(k,t)$) becomes $|\mathrm{B}_k(t)|$.

In equilibrium the mean-field theory yields the following conditions. For the type 1 phonons,

$$P = 0, \quad X = -\frac{4g}{\omega_0}\mathrm{Re}\phi, \tag{8}$$

and, for the type 2 phonons,

$$P_2 = 0, \quad X_2 = -\frac{2g_2}{\omega_2}\Delta n. \tag{9}$$

Here we note that since we are mainly interested in the electron dynamics, we only need the information on the average phonon displacement in the mean-field description. General quantities such as phonon occupations still depend on temperature, but here we do not need this information.

As for the electrons, by diagonalizing the mean-field Hamiltonian, Eq. (6a), and evaluating the expectation values of physical quantities from the thermally occupied eigenstates, we obtain the self-consistency relation

$$\phi = \frac{1}{N}\sum_k \frac{B^x_k + iB^y_k}{2B_k}[f(E_+(k),T) - f(E_-(k),T)], \tag{10a}$$

$$\Delta n = \frac{1}{N}\sum_k \frac{B^z_k}{B_k}[f(E_+(k),T) - f(E_-(k),T)], \tag{10b}$$

$$n_0 + n_1 = \frac{1}{N}\sum_k [f(E_+(k),T) + f(E_-(k),T)]. \tag{10c}$$

Here the components of the pseudo-magnetic field are

$$B^x_k = -2(U + 2\lambda)\mathrm{Re}\phi, \tag{11a}$$
$$B^y_k = -2U\mathrm{Im}\phi, \tag{11b}$$
$$B^z_k = 2\epsilon_{k,z} - (U + 2\lambda_2)\,\Delta n, \tag{11c}$$
$$B_k = \sqrt{(B^x_{\mathrm{k}})^2 + (B^y_{\mathrm{k}})^2 + (B^z_{\mathrm{k}})^2}, \tag{11d}$$

and $E_\pm(k) \equiv (\pm B_k + C^0_k)/2$. The Fermi distribution function at the temperature T is $f(\epsilon,T) = 1/(e^{\epsilon/T}+1)$. Without the type 1 el-ph coupling ($g = 0$), we can choose an arbitrary phase of the order parameter ϕ, while for $g \neq 0$, the order parameter ϕ becomes real and the remaining degree of freedom is its sign.

We also show the expression for the Green's functions since we use it in the next section. The lesser and greater parts of the Green's functions are defined as $G^<_{k,\alpha,\beta}(t,t') \equiv i\langle\hat{c}^\dagger_{k,\beta}(t')\hat{c}_{k,\alpha}(t)\rangle$ and $G^>_{k,\alpha,\beta}(t,t') \equiv -i\langle\hat{c}_{k,\alpha}(t)\hat{c}^\dagger_{k,\beta}(t')\rangle$ and we can regard them as 2×2 matrices in terms of the band index. In equilibrium within the mean-field theory with real order parameter, they are expressed as

$$\hat{G}^<_k(t) = \frac{i}{2}\sum_{\alpha=\pm} f(E_\alpha(k),T)e^{-iE_\alpha(k)t}\hat{M}_\alpha(k), \tag{12a}$$

$$\hat{G}^>_k(t) = -\frac{i}{2}\sum_{\alpha=\pm}(1 - f(E_\alpha(k),T))e^{-iE_\alpha(k)t}\hat{M}_\alpha(k), \tag{12b}$$

where

$$\hat{M}_{\pm}(k) = \pm\frac{B_k^x}{B_k}\hat{\sigma}_1 \pm \frac{B_k^z}{B_k}\hat{\sigma}_3 + \hat{\sigma}_0. \tag{13}$$

Additional study of susceptibilities

The dynamical susceptibilities evaluated from the mean-field dynamics correspond to those evaluated within the random phase approximation (RPA). In this section, we discuss this point in detail and show additional results for the susceptibility for the phase direction of the excitonic order parameter.

First, we consider the following four types of external homogeneous perturbations

$$\hat{H}_{\mathrm{ex},\nu}(t) = \delta F_{\mathrm{ex},\nu}(t)\sum_k \hat{\Psi}_k^\dagger \hat{\sigma}_\nu \hat{\Psi}_k, \tag{14}$$

where $\nu = 0,1,2,3$ and $\hat{\sigma}_\nu$ denotes the Pauli matrix. We also introduce $\hat{\rho}_\mu \equiv \frac{1}{N}\sum_k \hat{\Psi}_k^\dagger \hat{\sigma}_\mu \hat{\Psi}_k$. In the linear response regime, we can define the (full) susceptibility, $\chi^R_{\mu\nu}(t,\bar{t})$, as

$$\delta\langle\hat{\rho}_\mu(t)\rangle = \sum_\nu \int d\bar{t}\chi^R_{\mu\nu}(t,\bar{t})\delta F_{\mathrm{ex},\nu}(\bar{t}). \tag{15}$$

$\chi^R_{\mu\nu}$ detects collective modes with zero momentum. When the order parameter ϕ is taken real, $\langle\hat{\rho}_1(t)\rangle$ denotes the dynamics along the amplitude direction, while $\langle\hat{\rho}_2(t)\rangle$ corresponds to that along the phase direction of the order parameter. Therefore, if there is no mixing between the amplitude and the phase, χ^R_{11} and χ^R_{22} can be used to detect the amplitude mode and the phase mode, respectively [2].

Now we consider the expression of $\chi^R_{\mu\nu}$, which corresponds to the mean-field dynamics. We can rewrite the mean-field Hamiltonians as

$$H^{\mathrm{MF}}_{\mathrm{el}}(t) = H^{\mathrm{MF}}_{\mathrm{el,eq}} + \sum_{i,\nu}(\delta F_{\mathrm{ex},\nu}(t) + \delta F_\nu(t))\hat{\rho}_\nu, \tag{16a}$$

$$H^{\mathrm{MF}}_{\mathrm{ph0}}(t) = H^{\mathrm{MF}}_{\mathrm{ph0,eq}} + \delta H_0(t)\sum_i \hat{X}_i, \tag{16b}$$

$$H^{\mathrm{MF}}_{\mathrm{ph2}}(t) = H^{\mathrm{MF}}_{\mathrm{ph2,eq}} + \delta H_2(t)\sum_i \hat{X}_{i,2}. \tag{16c}$$

Here $H^{\mathrm{MF}}_{\mathrm{eq}}$ represents the mean-field Hamiltonians in equilibrium. $\delta F_\nu(t), \delta H_0(t)$ and $\delta H_2(t)$ are the changes in the mean-fields relative to the equilibrium values,

$$\delta F_\nu(t) = U_\nu \delta\langle\hat{\rho}_\nu(t)\rangle + \delta_{\nu,1} g\delta X(t) + \delta_{\nu,3} g_2 \delta X_2(t), \tag{17a}$$

$$\delta H_0(t) = g\delta\langle\hat{\rho}_1(t)\rangle, \tag{17b}$$

$$\delta H_2(t) = g_2\delta\langle\hat{\rho}_3(t)\rangle, \tag{17c}$$

with $[U_0,U_1,U_2,U_3] = [-U/2,U/2,U/2,U/2]$. Here $\delta\langle\hat{\rho}_\nu(t)\rangle$, $\delta X(t)$ and $\delta X_2(t)$ denote the difference from the equilibrium values.

In the linear response regime, from the standard Kubo formula and Eq. (16),

$$\delta\langle\hat{\rho}_\mu(t)\rangle = \sum_\nu \int d\bar{t}\chi^R_{0,\mu\nu}(t,\bar{t})[\delta F_{\mathrm{ex},\nu}(\bar{t}) + \delta F_\nu(\bar{t})], \tag{18a}$$

$$\delta X_0(t) = \int d\bar{t} D_0^R(t,\bar{t})\delta H_0(\bar{t}), \tag{18b}$$

$$\delta X_2(t) = \int d\bar{t} D_2^R(t,\bar{t})\delta H_2(\bar{t}). \tag{18c}$$

Here, χ_0^R is the susceptibility computed with the mean-field Hamiltonian with the mean-field fixed to the equilibrium value. It corresponds to bubble diagrams in the language of Feynman diagrams,

$$\chi^R_{0,\mu\nu}(t) = -i\theta(t)\frac{1}{N}\sum_k\Big\{\mathrm{tr}[\hat{\sigma}_\mu \hat{G}_k^>(t)\hat{\sigma}_\nu\hat{G}_k^<(-t) - \mathrm{tr}[\hat{\sigma}_\mu\hat{G}_k^<(t)\hat{\sigma}_\nu\hat{G}_k^>(-t)]\Big\}. \tag{19}$$

$D_0^R(t,t') \equiv -i\theta(t-t')\langle[\hat{X}_0(t),\hat{X}_0(t')]\rangle_0$ and $D_2^R(t,t') \equiv -i\theta(t-t')\langle[\hat{X}_2(t),\hat{X}_2(t')]\rangle_0$ are the retarded parts of the free phonon Green's functions for the type 1 and type 2 phonons, respectively. $\theta(t-t')$ is the Heaviside step function. By substituting Eq. (17) into Eq. (18), we obtain the self-consistent equation for $\delta\langle\hat{\rho}_\nu(t)\rangle$ expressed with $\chi^R_{0,\mu\nu}, D_0^R$ and D_2^R. We compare it with Eq. (15) and apply the Fourier transformation. This leads to a 4×4 system of equations for the susceptibility $\chi_{\mu\nu}$ in the following form

$$\hat{\chi}^R(\omega) = \hat{\chi}_0^R(\omega) + \hat{\chi}_0^R(\omega)\hat{\Theta}(\omega)\hat{\chi}^R(\omega), \tag{20}$$

where we have identified the irreducible vertex part

$$\hat{\Theta}(\omega) = \begin{bmatrix} \frac{U}{2} & 0 & 0 & 0 \\ 0 & -\frac{U}{2} + g^2 D_0^R(\omega) & 0 & 0 \\ 0 & 0 & -\frac{U}{2} & 0 \\ 0 & 0 & 0 & -\frac{U}{2} + g_2^2 D_2^R(\omega) \end{bmatrix}. \tag{21}$$

Here we note that the components $\chi^R_{0\nu}$ are zero since no perturbation considered here changes the total number of electrons. The external field proportional to the total number of electrons does not alter the dynamics, since it commutes with the Hamiltonian, and therefore $\chi^R_{\mu 0}$ are zero. From this consideration one can also see that the bare susceptibilities $\chi^R_{0,0\nu}$ and $\chi^R_{0,\mu 0}$ are zero. Therefore, in practice, we only need to focus on $\mu,\nu = 1,2,3$ in Eq. (20) and Eq. (21).

From Eq. (12), the bare susceptibility is given by

$$\chi^R_{0,\mu\nu}(t) = \theta(t)(-i\frac{1}{N})\sum_k\sum_{a=\pm}\frac{f(E_{\bar{a}}(k))-f(E_a(k))}{4} \times e^{-i(E_a(k)-E_{\bar{a}}(k))t}\mathrm{tr}[\hat{\sigma}_\mu\hat{M}_a\hat{\sigma}_\nu\hat{M}_{\bar{a}}] \quad (22)$$

and its Fourier transform yields a generalization of the Linhard formula

$$\hat{\chi}^R_0(\omega) = \frac{1}{N}\sum_k\frac{f(E_-(k),T)-f(E_+(k),T)}{4} \times\left(\frac{\hat{A}_k}{\omega^+-(E_+(k)-E_-(k))}-\frac{\hat{A}^T_k}{\omega^++(E_+(k)-E_-(k))}\right),$$

where $\omega^+=\omega+i\eta$, and the matrices $\hat{A}_k$ are obtained by the evaluation of $\mathrm{tr}[\hat{\sigma}_\mu\hat{M}_a\hat{\sigma}_\nu\hat{M}_{\bar{a}}]$:

$$\hat{A}_k = 4\begin{bmatrix}(\frac{B^z_k}{B_k})^2 & -i\frac{B^z_k}{B_k} & \frac{B^x_kB^z_k}{B^2_k}\\ i\frac{B^z_k}{B_k} & 1 & i\frac{B^x_k}{B_k}\\ \frac{B^x_kB^z_k}{B^2_k} & -i\frac{B^x_k}{B_k} & (\frac{B^x_k}{B_k})^2\end{bmatrix}. \quad (23)$$

From these expressions, one can see that the amplitude oscillations (represented by the 11 component) can be coupled to the phase oscillations. For example, let us take the parameter set used in the main text, which is in the BEC regime. Since $E_+(k)>0$ and $E_-(k)<0$ for all k,

$$\chi^R_{0,12}(t) = \theta(t)\frac{-2}{N}\sum_k\frac{B^z_k}{B_k}\cos(B_kt), \quad (24a)$$

$$\chi^R_{0,12}(\omega) = \frac{-2i}{N}\sum_k\frac{B^z_k}{B_k}\frac{\omega^+}{(\omega^+)^2-(E_+(k)-E_-(k))^2}. \quad (24b)$$

Since B^z_k/B_k is always positive there, this term does not vanish, in particular at finite ω, which leads to the mixing between amplitude and phase oscillations. This is in sharp contrast to the case of BCS superconductors, where the amplitude oscillations are decoupled from other components [2].

In Fig. 3, we compare the imaginary parts of the susceptibilities for the amplitude direction and the phase direction of the excitonic order parameter ($-\mathrm{Im}\chi^R_{11}(\omega)$ and $-\mathrm{Im}\chi^R_{22}(\omega)$) for the same parameter set as in the main text. Here $\chi^R_{\mu\mu}(\omega)$ is obtained by the Fourier transformation of $\chi^R_{\mu\mu}(t)$, which we directly measure by putting a field as defined in Eq. (14). We can see that the peaks in $-\mathrm{Im}\chi^R_{11}(\omega)$ and $-\mathrm{Im}\chi^R_{22}(\omega)$ emerge at the same positions. This means that the amplitude and phase oscillations are coupled. However, the mode which emerges from zero as we increase λ has larger intensity in $-\mathrm{Im}\chi^R_{22}(\omega)$ than in $-\mathrm{Im}\chi^R_{11}(\omega)$. This indicates that this mode is more related to the oscillations of the phase of the order parameter

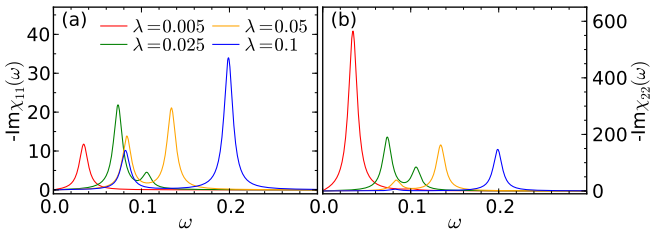

FIG. 3: (a) Imaginary part of the susceptibility for the amplitude direction of the excitonic order parameter ($-\mathrm{Im}\chi^R_{11}(\omega)$). (b) Imaginary part of the susceptibility for the phase direction of the excitonic order parameter ($-\mathrm{Im}\chi^R_{22}(\omega)$). We use the same parameters as in the main text ($\lambda_2=0$). The frequency dependent quantities $-\mathrm{Im}\chi^R(\omega)$ are numerically obtained from a Fourier transformation of $\chi^R_{\mu\mu}(t)$ with a damping factor $e^{-\eta t}$ and $\eta=0.006$.

than to those of the amplitude of the order parameter. One can also confirm this claim by observing $\chi^R_{21}(t)$ (not shown).

Dynamical phase transition

In Fig. 2(d) of the main text, we have shown the λ-dependence of the time-averaged order parameter ($\overline{|\phi(t)|}$), and we observed a sudden change in $\overline{|\phi(t)|}$ at some critical value λ_c at $E_0=0.12$. Here we show that this is associated with a qualitative change in the trajectory of the order parameter after the pump, see Figs. 4 (a)(b). To see this, let us fix the pump strength and change the el-ph coupling. When the el-ph coupling is small, the U(1) symmetry of the Hamiltonian is weakly broken and the free energy along the phase direction of the order parameter is almost flat. Therefore, the order parameter, as well as (B^x,B^y), can still rotate, see the result of $\lambda=0.002875$ in Figs. 4 (a)(b). For stronger el-ph coupling, however, the potential barrier becomes higher and the order parameter cannot rotate, see the result of $\lambda=0.003$ in Figs. 4(a)(b). This change in the trajectory gives rise to the sudden change of $\overline{|\phi(t)|}$ at $E_0=0.12$, which can be regarded as a dynamical phase transition. In general the trajectory around the transition between the different types of dynamics can be more involved with transient trappings in the potential minima, which manifests itself as a spiky structure in the result for $E_0=0.18$ in Fig. 2(d) of the main text.

We note that the dynamical phase transition manifests itself also in other quantities such as the phonon displacement X (see Figs. 4(c)(d)) and the gap (not shown). The sudden change in the time average of $X(t)$ is associated with the change of the trajectory as in the case of $\phi(t)$. When the el-ph coupling is sufficiently weak $X(t)$ oscillates between positive and negative sector. On the other hand, with stronger el-ph couplings, $X(t)$ is confined to the sector characterized by the same sign as in the initial

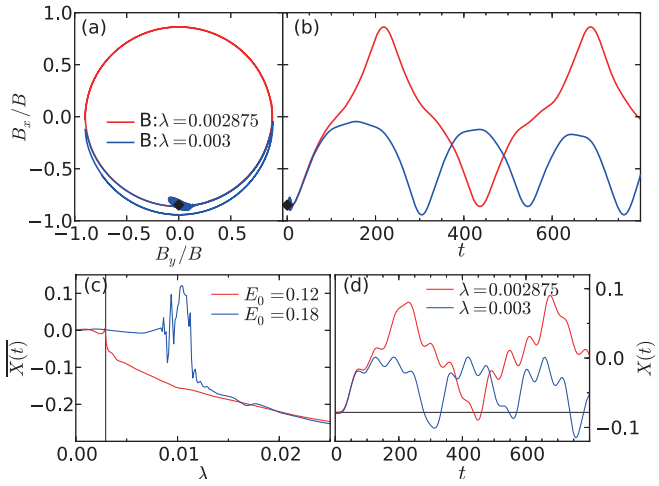

FIG. 4: (a)(b) Trajectory of the pseudo-magnetic field at $k = 0$ around λ_c (the jump) in Fig. 2(d) of the main text at $E_0 = 0.12$. (c) λ-dependence of the phonon displacement ($X(t)$) averaged over $t \in [0, 400]$. (d) Time evolution of $X(t)$ around λ_c (the jump) for $E_0 = 0.12$. The horizontal line indicates the equilibrium value. The parameters of the system and the pump condition are the same as in Fig. 2(d) in the main text.

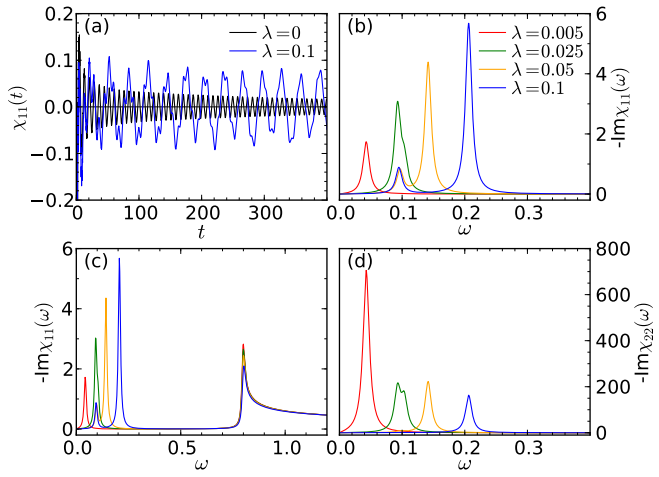

FIG. 5: Susceptibility (χ^R_{11}) in time ((a)) and frequency ((b)(c)) space for various cases with and without phonons for the set 2 parameters. (d) Imaginary part of the susceptibility for the phase direction of the excitonic order parameter ($-\mathrm{Im}\chi^R_{22}(\omega)$) for the same condition. The frequency-dependent quantities $-\mathrm{Im}\chi^R(\omega)$ are obtained from a Fourier transformation of $\chi^R(t)$ with a damping term $e^{-\eta t}$ and $\eta = 0.006$.

state (in the present case negative).

Dynamics in the BEC-BCS crossover regime

In the previous experimental literature on Ta_2NiSe_5 [3], different model parameters have been extracted from a different ARPES measurement. Here we show that also for parameters different from those used in the main text the proposed mechanism for the photo-enhanced condensate can remain valid.

In the main text, we used the parameters extracted from Ref. 4. For this parameter set the system is on the BEC side within the mean-field theory, since B^z_k is positive in the EI phase for all k . On the other hand in Ref. 3, the ARPES spectra show an upturn of the valence band in the EI. In order to explain this, parameters closer to the BCS-BEC crossover have been considered. The parameters from Ref. 3 are $\Delta_0 = 0.05, \Delta_1 = -2.15, U = 2.1$, and $\lambda = 0$. We will use these values, which we will refer to as "set 2 parameters", as reference parameters below, and adjust the $\Delta_{0,1}$ and U for $\lambda > 0$ as explained in the main text. We consider $T = 0$ and $\omega_0 = 0.1$ and repeat the same analysis as in the main text. For this parameter set and within the mean-field analysis, B^z_k is negative around $k = 0$ in the EI phase, and positive elsewhere. In this sense, we may say that this is in the BCS regime at least at $T = 0$. The negative B^z_k around $k = 0$ leads to the upturn structure in the quasiparticle spectrum, hence the minimum band gap Δ_{EI} is now located away from $k = 0$. This is consistent with the upturn in the ARPES spectrum. We note that if the difference in the band occupancy $|\Delta n|$ is 1, which is its maximum value, the Hartree shift is $-U\Delta n = U$, and B^z_k is positive everywhere for the set 2 parameters. However in the EI phase $|\Delta n| < 1$ and this does not happen.

In Fig. 5, we show $\chi^R_{11}(t)$ for the model with and without phonons. Without phonons, there emerge prominent oscillations with the frequency of $\Delta_{\mathrm{EI}} = 0.80$. In contrast to the result in the main text, the damping of the oscillations is well described by a power law $1/t^{0.5}$, which is consistent with the mean-field prediction for superconductors in the BCS regime [5–8]. This fact shows that whether B^z_k changes sign along k in the EI phase has a crucial effect on the decay of the amplitude mode. In Figs. 5(b-d), we show the imaginary part of the susceptibilities $-\mathrm{Im}\chi^R_{11}(\omega)$ and $-\mathrm{Im}\chi^R_{22}(\omega)$. With the el-ph coupling, as in the case in the main text, two additional types of collective oscillations emerge, which originate from the massive phase mode and the phonon. The general features of these two modes are the same as in the main text. The main difference in $-\mathrm{Im}\chi^R_{11}(\omega)$ is the peak and the continuum above $\omega = \Delta_{\mathrm{EI}}$, which appears because the amplitude mode with frequency Δ_{EI} is now prominent and decays slowly.

We further note that if the system would be on the verge of the BCS-BEC crossover, one may be able to either reveal or suppress the amplitude mode with the frequency Δ_{EI} by slightly changing the system by, for example, applying pressure or chemical intercalation.

Now we look at the nonequilibrium dynamics after a pump pulse. Here we use the same condition for the pump as in the main text. In Fig. 6, we show the results for the set 2 parameters, which can be compared

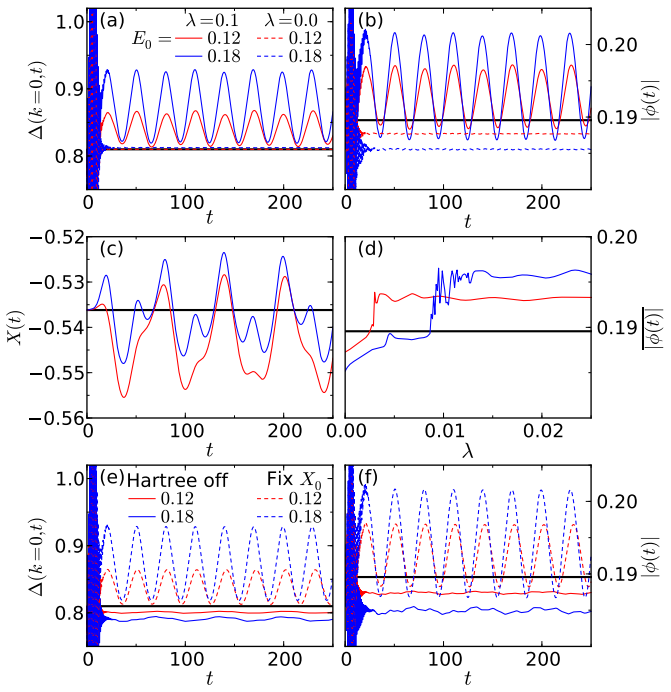

FIG. 6: (a-c) Time evolution of the gap at $k = 0$ ($\Delta(k = 0, t)$), the excitonic order parameter ($|\phi|$), and the phonon displacement (X) for various field strengths and el-ph couplings. (d) The dependence of the size of the order parameter averaged over $t \in [0, 400]$ for various field strengths. (e,f) $\Delta(k = 0, t)$, $|\phi|$ for $\lambda = 0.1$ evaluated by freezing the Hartree shift (solid lines) and the phonon displacement (dashed lines). We have used the set 2 parameters as a reference (see the text).

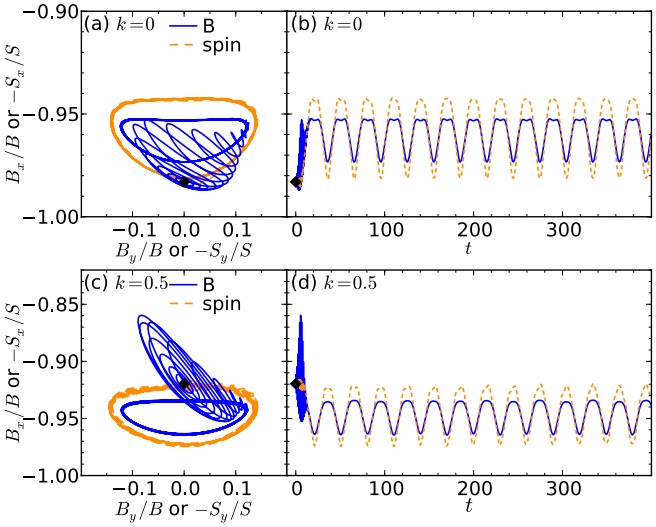

FIG. 7: (a) The trajectory of $(B^x/B, B^y/B)$ and $(-S^x/S, -S^y/S)$ (b) and the time evolution of B^x/B and $-S^x/S$ at $k = 0$ for $\lambda = 0.1$. (c) The trajectory of $(B^x/B, B^y/B)$ and $(-S^x/S, -S^y/S)$ (d) and the time evolution of B^x/B and $-S^x/S$ at $k = 0.5$ for $\lambda = 0.1$. We used the set 2 parameters as a reference condition, and the parameters $t_p = 6.0$ and $E_0 = 0.12$ for the laser excitation.

to Fig. 2 in the main text. With the el-ph coupling, we can again see an enhancement of the EI order ($|\phi|$), the displacement of the phonons (X) and the gap at $k = 0$ ($\Delta(k = 0, t)$). We also confirm that without the Hartree shift there is no enhancement, see Fig. 6(e)(f). A positive feedback from the dynamics of phonons exists for small E_0 (compare the full case and the case with X fixed). This effect can be also seen more prominently in the parameter used in the main text (not shown).

Without the el-ph coupling, $|\phi|$ decreases after the pump, while $\Delta(k = 0, t)$ remains almost at the same position. This originates from $B^z_{k=0}$ being negative: After the photo-doping $B^z_{k=0}$ becomes even more negative due to the modified Hartree shift. Since the gap corresponds to the magnitude of the pseudo-magnetic field (see the explanation around Eq. (11d)), this enhancement of $|B_z|$ and the decrease of the order parameter (which is reflected in $B_{x,y}$) have opposite effects on the size of the gap and compensate each other.

Next we show how the pseudo-magnetic field and the pseudo-spin evolve in the present case. First we note that $B^z_{k=0}$ is negative and it becomes more negative after the pump. Therefore, the magnetic field is less tilted along the xy direction and we can expect a decrease of $|S^x_k + iS^y_k|$. This is indeed the case as is depicted in Fig. 7(a)(b). On the other hand, away from $k = 0$, B^z becomes positive in equilibrium and the mechanism mentioned in the main text is applicable again. As is shown in Fig. 7(c)(d), one can see that there is indeed an enhancement of $|S^x_k + iS^y_k|$ away from $k = 0$. For the set 2 parameters, the region around $k = 0$ and that away from $k = 0$ therefore give negative and positive contributions to the EI order after the pump, respectively, but in total the positive contribution dominates and the EI order is enhanced. Hence, the mechanism discussed in the main text also holds for the present choice of parameters.

Finally, we show the trARPES spectrum in Fig. 8. This corresponds to Fig. 4 of the main text. Before the excitation, we can see the slight upturn in the dispersion, see Fig. 8(a). This originates from B^z_k being negative around $k = 0$. After the pump pulse, the band shifts away from the Fermi level around $k = 0$, while it shifts toward the Fermi level away from $k = 0$. As a result the upturn becomes more prominent, see Fig. 8(b). In Fig. 8(c), we show $\delta\Delta_{\rm ARPES}(k, t_{\rm pr})$, the time evolution of the difference between the equilibrium and nonequilibrium band gap at each k. One can again see the decrease of the band distance around $k = 0$, and the increase away from $k = 0$. As can be seen from $\delta\Delta_{\rm ARPES}(0, t_{\rm pr})$, the band position oscillates with the frequency of the collective modes.

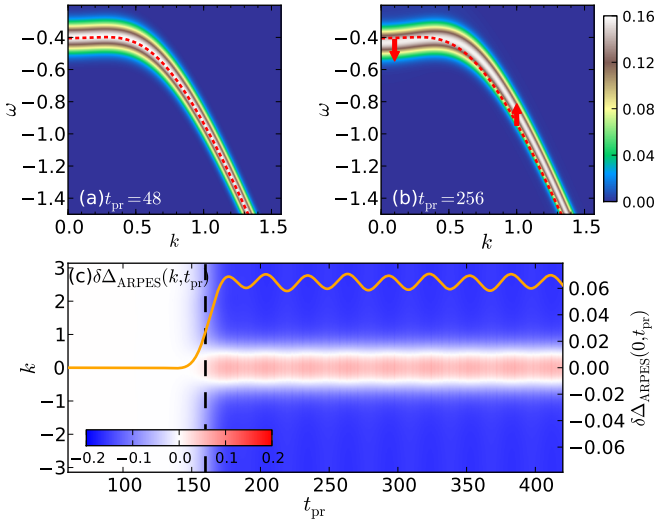

FIG. 8: (a)(b) Time-resolved ARPES spectra derived from the retarded part of the Green's functions ($A^R_k(\omega;t_{\rm pr})$) before (a) and after (b) the laser pump. Red dashed lines indicate the equilibrium quasiparticle dispersion from the mean-field theory. (c) Time evolution of the difference between the equilibrium and nonequilibrium gap size at each momentum k ($\delta\Delta_{\rm ARPES}(k,t_{\rm pr})$), see the text. The orange solid line is $\delta\Delta_{\rm ARPES}(0,t_{\rm pr})$ (axis on the right). The parameters are $\lambda = 0.1$ with $E_0 = 0.18$, $\sigma_{\rm p} = 3.0$, $\Omega = 6.0$, $t_{\rm p} = 160.0$, and $\sigma_{\rm pr} = 12.0$. The black dashed line indicates the center of the pump pulse.

[1] D. Werdehausen *et al.*, arXiv:1611.01053 (2016).
[2] I. Kulik, O. Entin-Wohlman, and R. Orbach, J. Low Temp. Phys. **43**, 591 (1981).
[3] K. Seki *et al.*, Phys. Rev. B **90**, 155116 (2014).
[4] S. Mor *et al.*, Phys. Rev. Lett. **119**, 086401 (2017).
[5] A. Volkov and S. Kogan, Sov. Phys. JETP **38**, 1018 (1974).
[6] E. A. Yuzbashyan, O. Tsyplyatyev, and B. L. Altshuler, Phys. Rev. Lett. **96**, 097005 (2006).
[7] R. A. Barankov and L. S. Levitov, Phys. Rev. Lett. **96**, 230403 (2006).
[8] E. A. Yuzbashyan and M. Dzero, Phys. Rev. Lett. **96**, 230404 (2006).